

# World Journal of *Gastroenterology*

*World J Gastroenterol* 2022 August 7; 28(29): 3753-4018



**REVIEW**

- 3753 Mechanistic and functional extrapolation of SET and MYND domain-containing protein 2 to pancreatic cancer  
*Alshammari E, Zhang YX, Yang Z*

**MINIREVIEWS**

- 3767 Clinical challenge for gastroenterologists–Gastrointestinal manifestations of systemic mastocytosis: A comprehensive review  
*Elvevi A, Elli EM, Lucà M, Scaravaglio M, Pagni F, Ceola S, Ratti L, Invernizzi P, Massironi S*
- 3780 Structural changes of proteins in liver cirrhosis and consequential changes in their function  
*Gligorijević N, Minić S, Nedić O*
- 3793 Epidemiologic and socioeconomic factors impacting hepatitis B virus and related hepatocellular carcinoma  
*Gnyawali B, Pusateri A, Nickerson A, Jalil S, Mumtaz K*
- 3803 Endoscopic salvage therapy after failed biliary cannulation using advanced techniques: A concise review  
*Tsou YK, Pan KT, Lee MH, Lin CH*
- 3814 Enhanced endoscopic ultrasound imaging for pancreatic lesions: The road to artificial intelligence  
*Spadaccini M, Koleth G, Emmanuel J, Khalaf K, Facciorusso A, Grizzi F, Hassan C, Colombo M, Mangiavillano B, Fugazza A, Anderloni A, Carrara S, Repici A*

**ORIGINAL ARTICLE****Basic Study**

- 3825 Qingyi decoction attenuates intestinal epithelial cell injury *via* the calcineurin/nuclear factor of activated T-cells pathway  
*Wang GY, Shang D, Zhang GX, Song HY, Jiang N, Liu HH, Chen HL*
- 3838 High-fat diet aggravates colitis *via* mesenteric adipose tissue derived exosome metastasis-associated lung adenocarcinoma transcript 1  
*Chen D, Lu MM, Wang JH, Ren Y, Xu LL, Cheng WX, Wang SS, Li XL, Cheng XF, Gao JG, Kalyani FS, Jin X*
- 3854 Involvement of nitrergic neurons in colonic motility in a rat model of ulcerative colitis  
*Li YR, Li Y, Jin Y, Xu M, Fan HW, Zhang Q, Tan GH, Chen J, Li YQ*
- 3869 N-linked glycoproteomic profiling in esophageal squamous cell carcinoma  
*Liu QW, Ruan HJ, Chao WX, Li MX, Jiao YL, Ward DG, Gao SG, Qi YJ*

- 3886** HP0953 - hypothetical virulence factor overexpression and localization during *Helicobacter pylori* infection of gastric epithelium

*Arteaga-Resendiz NK, Rodea GE, Ribas-Aparicio RM, Olivares-Cervantes AL, Castelán-Vega JA, Olivares-Trejo JJ, Mendoza-Elizalde S, López-Villegas EO, Colín C, Aguilar-Rodea P, Reyes-López A, Salazar García M, Velázquez-Guadarrama N*

- 3903** Involvement of toll-like receptor 5 in mouse model of colonic hypersensitivity induced by neonatal maternal separation

*Mallaret G, Lashermes A, Meleine M, Boudieu L, Barbier J, Aissouni Y, Gelot A, Chassaing B, Gewirtz AT, Ardid D, Carvalho FA*

#### Case Control Study

- 3917** Comprehensive evaluation of microRNA as a biomarker for the diagnosis of hepatocellular carcinoma

*Malik J, Klammer M, Rolny V, Chan HLY, Piratvisuth T, Tanwandee T, Thongsawat S, Sukeepaisarnjaroen W, Esteban JJ, Bes M, Köhler B, Swiatek-de Lange M*

#### Retrospective Cohort Study

- 3934** Optimal timing of biliary drainage based on the severity of acute cholangitis: A single-center retrospective cohort study

*Lu ZQ, Zhang HY, Su CF, Xing YY, Wang GX, Li CS*

#### Retrospective Study

- 3946** Incidence and clinical characteristics of hypertriglyceridemic acute pancreatitis: A retrospective single-center study

*Lin XY, Zeng Y, Zhang ZC, Lin ZH, Chen LC, Ye ZS*

- 3960** Radiomics for differentiating tumor deposits from lymph node metastasis in rectal cancer

*Zhang YC, Li M, Jin YM, Xu JX, Huang CC, Song B*

- 3971** Effects of microwave ablation on serum Golgi protein 73 in patients with primary liver cancer

*Xu ZJ, Wei MJ, Zhang XM, Liu HG, Wu JP, Huang JF, Li YF, Huang ZJ, Yan YY*

#### Observational Study

- 3981** Evaluating the best treatment for multifocal hepatocellular carcinoma: A propensity score-matched analysis

*Risaliti M, Bartolini I, Campani C, Arena U, Xodo C, Adotti V, Rosi M, Taddei A, Muiasan P, Amedei A, Batignani G, Marra F*

- 3994** Structure of the myenteric plexus in normal and diseased human ileum analyzed by X-ray virtual histology slices

*Veress B, Peruzzi N, Eckermann M, Frohn J, Salditt T, Bech M, Ohlsson B*

#### META-ANALYSIS

- 4007** Recurrence rates after endoscopic resection of large colorectal polyps: A systematic review and meta-analysis

*Rotermund C, Djinbachian R, Taghiakbari M, Enderle MD, Eickhoff A, von Renteln D*

**ABOUT COVER**

Editorial Board Member of *World Journal of Gastroenterology*, Nikolaos Papadopoulos, MD, PhD, Consultant, The First Department of Internal Medicine, 417 Army Share Fund Hospital, Monis Petraki 10-12, Athens 11521, Greece. nipapmed@gmail.com

**AIMS AND SCOPE**

The primary aim of *World Journal of Gastroenterology* (*WJG, World J Gastroenterol*) is to provide scholars and readers from various fields of gastroenterology and hepatology with a platform to publish high-quality basic and clinical research articles and communicate their research findings online. *WJG* mainly publishes articles reporting research results and findings obtained in the field of gastroenterology and hepatology and covering a wide range of topics including gastroenterology, hepatology, gastrointestinal endoscopy, gastrointestinal surgery, gastrointestinal oncology, and pediatric gastroenterology.

**INDEXING/ABSTRACTING**

The *WJG* is now abstracted and indexed in Science Citation Index Expanded (SCIE, also known as SciSearch®), Current Contents/Clinical Medicine, Journal Citation Reports, Index Medicus, MEDLINE, PubMed, PubMed Central, Scopus, Reference Citation Analysis, China National Knowledge Infrastructure, China Science and Technology Journal Database, and Superstar Journals Database. The 2022 edition of Journal Citation Reports® cites the 2021 impact factor (IF) for *WJG* as 5.374; IF without journal self cites: 5.187; 5-year IF: 5.715; Journal Citation Indicator: 0.84; Ranking: 31 among 93 journals in gastroenterology and hepatology; and Quartile category: Q2. The *WJG*'s CiteScore for 2021 is 8.1 and Scopus CiteScore rank 2021: Gastroenterology is 18/149.

**RESPONSIBLE EDITORS FOR THIS ISSUE**

Production Editor: *Ying-Yi Yuan*; Production Department Director: *Xiang Li*; Editorial Office Director: *Jia-Ru Fan*.

**NAME OF JOURNAL**

*World Journal of Gastroenterology*

**ISSN**

ISSN 1007-9327 (print) ISSN 2219-2840 (online)

**LAUNCH DATE**

October 1, 1995

**FREQUENCY**

Weekly

**EDITORS-IN-CHIEF**

Andrzej S Tarnawski

**EDITORIAL BOARD MEMBERS**

<http://www.wjgnet.com/1007-9327/editorialboard.htm>

**PUBLICATION DATE**

August 7, 2022

**COPYRIGHT**

© 2022 Baishideng Publishing Group Inc

**INSTRUCTIONS TO AUTHORS**

<https://www.wjgnet.com/bpg/gerinfo/204>

**GUIDELINES FOR ETHICS DOCUMENTS**

<https://www.wjgnet.com/bpg/GerInfo/287>

**GUIDELINES FOR NON-NATIVE SPEAKERS OF ENGLISH**

<https://www.wjgnet.com/bpg/gerinfo/240>

**PUBLICATION ETHICS**

<https://www.wjgnet.com/bpg/GerInfo/288>

**PUBLICATION MISCONDUCT**

<https://www.wjgnet.com/bpg/gerinfo/208>

**ARTICLE PROCESSING CHARGE**

<https://www.wjgnet.com/bpg/gerinfo/242>

**STEPS FOR SUBMITTING MANUSCRIPTS**

<https://www.wjgnet.com/bpg/GerInfo/239>

**ONLINE SUBMISSION**

<https://www.f6publishing.com>

## Observational Study

# Structure of the myenteric plexus in normal and diseased human ileum analyzed by X-ray virtual histology slices

Bela Veress, Niccolò Peruzzi, Marina Eckermann, Jasper Frohn, Tim Salditt, Martin Bech, Bodil Ohlsson

**Specialty type:** Gastroenterology and hepatology**Provenance and peer review:**

Unsolicited article; Externally peer reviewed.

**Peer-review model:** Single blind**Peer-review report's scientific quality classification**Grade A (Excellent): 0  
Grade B (Very good): B  
Grade C (Good): C  
Grade D (Fair): 0  
Grade E (Poor): 0**P-Reviewer:** Goldstein AM, United States; Natale G, Italy**Received:** April 28, 2022**Peer-review started:** April 28, 2022**First decision:** May 11, 2022**Revised:** May 18, 2022**Accepted:** July 11, 2022**Article in press:** July 11, 2022**Published online:** August 7, 2022**Bela Veress**, Department of Pathology, Skåne University Hospital, Malmö 205 02, Sweden**Niccolò Peruzzi, Martin Bech**, Medical Radiation Physics, Department of Clinical Sciences, Lund University, Lund 221 00, Sweden**Marina Eckermann, Jasper Frohn, Tim Salditt**, Institute for X-Ray Physics, University of Göttingen, Göttingen 37077, Germany**Marina Eckermann, Tim Salditt**, Cluster of Excellence "Multiscale Bioimaging: from Molecular Machines to Networks of Excitable Cells" (MBExC), University of Göttingen, Göttingen 37077, Germany**Marina Eckermann**, ESRF, The European Synchrotron, Grenoble 38043, France**Bodil Ohlsson**, Department of Internal Medicine, Skåne University Hospital, Lund University, Malmö S-205 02, Sweden**Corresponding author:** Bodil Ohlsson, MD, PhD, Full Professor, Department of Internal Medicine, Skåne University Hospital, Lund University, 15 Jan Waldenströms Street, Malmö S-205 02, Sweden. [bodil.ohlsson@med.lu.se](mailto:bodil.ohlsson@med.lu.se)

## Abstract

### BACKGROUND

The enteric nervous system (ENS) is situated along the entire gastrointestinal tract and is divided into myenteric and submucosal plexuses in the small and large intestines. The ENS consists of neurons, glial cells, and nerves assembled into ganglia, surrounded by telocytes, interstitial cells of Cajal, and connective tissue. Owing to the complex spatial organization of several interconnections with nerve fascicles, the ENS is difficult to examine in conventional histological sections of 3-5  $\mu\text{m}$ .

### AIM

To examine human ileum full-thickness biopsies using X-ray phase-contrast nanotomography without prior staining to visualize the ENS.

### METHODS

Six patients were diagnosed with gastrointestinal dysmotility and neuropathy based on routine clinical and histopathological examinations. As controls, full-thickness biopsies were collected from healthy resection ileal regions after

hemicolectomy for right colon malignancy. From the paraffin blocks, 4- $\mu$ m thick sections were prepared and stained with hematoxylin and eosin for localization of the myenteric ganglia under a light microscope. A 1-mm punch biopsy (up to 1 cm in length) centered on the myenteric plexus was taken and placed into a Kapton<sup>®</sup> tube for mounting in the subsequent investigation. X-ray phase-contrast tomography was performed using two custom-designed laboratory setups with micrometer resolution for overview scanning. Subsequently, selected regions of interest were scanned at a synchrotron-based end-station, and high-resolution slices were reported. In total, more than 6000 virtual slices were analyzed from nine samples.

## RESULTS

In the overview scans, the general architecture and quality of the samples were studied, and the myenteric plexus was localized. High-resolution scans revealed details, including the ganglia, interganglionic nerve fascicles, and surrounding tissue. The ganglia were irregular in shape and contained neurons and glial cells. Spindle-shaped cells with very thin cellular projections could be observed on the surface of the ganglia, which appeared to build a network. In the patients, there were no alterations in the general architecture of the myenteric ganglia. Nevertheless, several pathological changes were observed, including vacuolar degeneration, autophagic activity, the appearance of sequestosomes, chromatolysis, and apoptosis. Furthermore, possible expulsion of pyknotic neurons and defects in the covering cellular network could be observed in serial slices. These changes partly corresponded to previous light microscopy findings.

## CONCLUSION

The analysis of serial virtual slices could provide new information that cannot be obtained by classical light microscopy. The advantages, disadvantages, and future possibilities of this method are also discussed.

**Key Words:** Enteric nervous system; Immunohistochemistry; Neuropathy; Synchrotron; Virtual histology; X-ray phase-contrast nanotomography

©The Author(s) 2022. Published by Baishideng Publishing Group Inc. All rights reserved.

**Core Tip:** Full-thickness biopsies of 1 mm diameter and up to 1 cm length from the human ileum were scanned using two laboratory-based  $\mu$ -computed tomography setups to study the architecture of the enteric nervous system (ENS) and further scanned by a synchrotron-based end-station for histopathological studies, without any staining. Several pathological neuronal changes, such as vacuolar degeneration, autophagic activity, appearance of sequestosomes, chromatolysis, and apoptosis, were identified in diseased patients. Phenomena that were undetectable by light microscopy were observed. The relationships among various tissue components could be followed in all directions. Thus, this method provides a unique analysis of the ENS.

**Citation:** Veress B, Peruzzi N, Eckermann M, Frohn J, Salditt T, Bech M, Ohlsson B. Structure of the myenteric plexus in normal and diseased human ileum analyzed by X-ray virtual histology slices. *World J Gastroenterol* 2022; 28(29): 3994-4006

**URL:** <https://www.wjgnet.com/1007-9327/full/v28/i29/3994.htm>

**DOI:** <https://dx.doi.org/10.3748/wjg.v28.i29.3994>

## INTRODUCTION

The neurons of the enteric nervous system (ENS) assemble into ganglia, forming the submucosal and myenteric plexuses[1]. The ganglia, which also contain glial cells, are connected by nerve fascicles and are surrounded by telocytes and interstitial cells of Cajal (ICC), as well as by other cells and fibers of connective tissue. Various diseases of the ENS may lead to severe bowel motility dysfunction in the form of chronic intestinal pseudo-obstruction (CIPO) and enteric dysmotility (ED)[2,3]. Enteric neuropathy is seldom studied because only a few centers are available for the evaluation of gastrointestinal motility, access to the myenteric plexus requires full-thickness bowel biopsies, and pathologists subspecializing in neuromuscular diseases of the ENS are scarce. Subsequently, the neuropathy diagnosis may be ignored or delayed for several years, which prevents proper healthcare of the patients[4].

We recently presented a methodology to use X-ray phase-contrast nanotomography to study the volume and structure of the ENS[5]. Neurons and surrounding structures are visible using this method without any prior staining, allowing the possibility to study large sample volumes[5,6]. The aim of the present qualitative analysis of virtual slices was to describe in detail the structure of human ileal myenteric ganglia in the normal human ileum as well as in patients with CIPO or ED.

## MATERIALS AND METHODS

### *Patients and samples*

Six patients with severe gastrointestinal pain and dysmotility were examined using esophageal manometry, gastric emptying scintigraphy, antroduodenjejunal manometry, and colonic transit time, after exclusion of organic disease. Patients were diagnosed with CIPO when they fulfilled the following three criteria: a medical history compatible with pseudo-obstruction, documented events or chronic signs mimicking mechanical obstruction (bowel dilatation and/or air/fluid levels), and absence of mechanical obstruction or other organic causes for these symptoms and findings[3]. The criteria for ED were documented abnormal contractile activity, but no history of episodes or current signs mimicking mechanical obstruction and the absence of any medication that could lead to the observed motor abnormalities[2].

A previously described laparoscopy-assisted technique for ileal full-thickness biopsies and the preparation of biopsies was used[4,7]. Briefly, 1.0 cm × 1.5 cm large full-thickness biopsies were cut from the ileum and embedded in paraffin. Transversal and horizontal 3-5-mm thick serial sections were stained according to the protocol for CIPO analysis[8]. Histopathological findings were evaluated by a pathologist (B.V.) and classified as previously described[9]. The criteria for neuropathies were based on criteria suggested by the Gastro 2009 International Working Group for Gastrointestinal Neuromuscular Pathology[10]. The histopathological diagnoses and various stains, such as CD117 for ICC, CD34 for telocytes, S100 for Schwann cells, periodic acid-Schiff (PAS) with or without diastase (PAS-D) for carbohydrates or their compounds (*e.g.*, glycogen and mucin), and p62 for sequestosome, were obtained from the medical records (Table 1). For all patients, the disease initially presented when they were adults without any known heredity. Genetic analysis was not performed. There was no correlation between the varying histopathological findings described in Table 1 and the clinical presentation or other functional findings of patients (data not shown).

Three men aged 45, 54, and 82 years were used as controls, all of whom had undergone hemicolectomy due to malignancy in the right colon. A full-thickness biopsy specimen was collected and stained from the healthy resection region of the ileum. The sample size was adopted based on the beam time available in the laboratory.

### *Sample preparation*

From the paraffin blocks of these nine individuals, 4- $\mu$ m thick sections were prepared and stained with hematoxylin and eosin (H&E) for the localization of the myenteric ganglia under a light microscope. A biopsy punch of 1 mm diameter and up to 1 cm in length centered on the myenteric plexus was taken from the paraffin blocks of patients and controls and placed into a Kapton® tube (Paramount, Indiana, United States) for mounting in the subsequent tomographic investigation[11].

### *X-ray phase-contrast tomography*

X-ray phase-contrast tomography was performed on two custom-designed laboratory setups with micrometer resolution, located at the Institute for X-Ray Physics, University of Göttingen, Göttingen, Germany[11] and a Gottingen Instrument for Nano-Imaging with X-rays (GINIX), installed at the P10/PETRAIII beamline (Hamburg, Germany) with sub-micron resolution[12]. All setups used propagation-based, phase-contrast methods, in which the sample is placed between the source and detector, and the phase information is obtained by free-space propagation and self-interference of the coherent X-ray beam without the need for additional optical elements. Phase retrieval is necessary to correctly extract phase information before tomographic reconstruction[13-15].

The two laboratory setups were installed at a liquid metal jet source (Excillum, Kista, Sweden) or a microfocus rotating anode (mm007, Rigaku, Austin, TX, United States). Both setups used high-resolution scintillator-based detectors (Xsight, Rigaku) and employed broad bandpass radiation peaking at the characteristic lines of Ga Ka (9.25 keV) and Cu (8.05 keV) for the liquid jet and rotating anode sources, respectively. Phase retrieval was performed using the Bronnikov-aided correction algorithm[11, 15,16]. As a result, these home-built setups allowed us to image the whole 1-mm wide and several-mm long sample with an isotropic effective voxel size of approximately 1  $\mu$ m (approximately 15 h scan time per sample), enabling identification of the neural tissue structure (further information about the experimental parameters is provided in Table 2). The two systems could run in parallel and were used to optimize time consumption.

**Table 1 Basic characteristics of subjects**

Age, sex	Disease (years)	Clinical diagnosis	Histopathological findings	Histopathological diagnosis	X-ray
45, M	NA	Control	Normal neurons	Healthy	Healthy
54, M	NA	Control	Normal neurons	Healthy	Healthy
82, M	NA	Control	Normal neurons	Healthy	Healthy
27, W	4	ED/type 1 diabetes	Vacuolated, apoptotic neurons, chromatolysis	Lymphocytic ganglioneuritis	Vacuolated, shrunken neurons, chromatolysis, autophagia
27, W	6	Idiopathic ED	Vacuolated neurons, chromatolysis	Degenerative neuropathy	Pre-apoptotic and dead nucleus
32, W	2	Drug-induced CIPO	Vacuolated, shrunken, chromatolysis, hyperplasia ICC	Visceral degenerative neuropathy with axon vacuolization, hyperplasia, and vacuolization of ICCs, and hypertrophy of the longitudinal and internal circular muscle layers	Only fascicle, no ganglia for evaluation
43, W	3	Idiopathic ED	Amphophilic shrunken neurons, Vacuolated neurons, chromatolysis	Lymphocytic ganglioneuritis with neurondegeneration	Amphophilic degeneration, vacuolated neurons
52, W	4	Idiopathic ED	Vacuolated, shrunken neurons, hypoplasia of ICC	Lymphocytic ganglioneuritis	Vacuolated, shrunken neurons, chromatolysis
56, W	50	ED/Ehlers-Danlos	Vacuolated neurons, chromatolysis, hyperplasia ICC	Lymphocytic ganglioneuritis with vacuolar neurodegeneration and hyperplasia of the ICC	Severe atrophy with reduced volume

Data obtained from the medical records; disease duration assessed in years. CIPO: Chronic intestinal pseudo-obstruction; ED: Enteric dysmotility; ICC: Interstitial cells of Cajal; M: Man; W: Woman; NA: Not available.

**Table 2 Experimental and reconstruction parameters**

Scan configuration	Effective pixel size ( $\mu\text{m}$ )	Energy (keV)	Number of projections <sup>1</sup>	Phase retrieval scheme	Phase retrieval parameter	Ring removal algorithm
Laboratory setup (liquid metal jet)	0.920 <sup>2</sup>	9.25 (K $\alpha$ )	1 × 1000 (50 s) or 1 × 700 (40 s)	BAC	$\alpha = 0.008, \beta = 0.160$	Wavelet
Laboratory setup (rotating anode)	1.072	8.05 (K $\alpha$ )	1 × 1000 (50 s) or 1 × 700 (40 s)	BAC	$\alpha = 0.07, \beta = 0.16$	Wavelet
GINIX waveguide (all samples except for ED/Ehlers-Danlos patient)	0.169	8.00	4 × 1500 (1 s) or 3 × 1500 (1 s)	Non-linear Tikhonov <sup>3</sup>	$\delta/\beta = 50, \text{lim1} = 8e-3, \text{lim2} = 0.5$	Additive
GINIX waveguide (ED/Ehlers-Danlos patient)	0.176	7.50	4 × 1000 (2 s)	Non-linear Tikhonov <sup>3</sup>	$\delta/\beta = 50, \text{lim1} = 1e-4, \text{lim2} = 0.1$	Additive

<sup>1</sup>Due to time constraints, some samples were scanned with a lower number of projections and shorter exposure times (in the overview scans) or with less distances (in the high-resolution scans of the drug-induced chronic intestinal pseudo-obstruction patient and of the 40 years old control).

<sup>2</sup>After voxel binning of  $2 \times 2 \times 2$ .

<sup>3</sup>No support, no restriction on phase shift.

GINIX: Gottingen Instrument for Nano-Imaging with X-rays; ED: Enteric dysmotility.

Selected regions of interest (ROIs) of  $320 \mu\text{m} \times 320 \mu\text{m} \times 320 \mu\text{m}$  were scanned with an isotropic effective voxel size of 169 nm at the synchrotron-based end-station (approximately 2.5-3.0 h scan time), using inline holography based on a coherent divergent beam [8 keV, Si (111) monochromator] exiting from an X-ray waveguide[11,12]. Holographic phase retrieval based on contrast-transfer-function (CTF) approach, ring removal, and tomographic reconstructions were performed using in-house reconstruction pipelines[16]. Further details can be found in Table 2.

Complete information regarding the experimental setups and reconstruction pipelines, which were performed by physicists unaware of the diagnosis, is provided in a previous publication[5]. The analysis of the slices reported in this paper was performed on the data acquired at the synchrotron end-station, on the high-resolution scans.

### Image analysis

All the obtained volumetric datasets were digitally sectioned along any arbitrary slicing plane, enabling virtual histology of the samples. In the histological evaluation, the term “spindle-shaped cells” was used to describe the cells around the ganglia, which represented either telocytes, ICCs, or fibroblasts/cytes because no differentiation could be made without immunohistochemistry. In cases where identification can be made from double immunohistochemical staining of the same regions[17], the cells are called telocytes or ICC. In total, more than 6000 virtual slices were analyzed from the nine samples.

## RESULTS

In the overview scans performed with the laboratory setup, the general architecture of the bowel samples was examined with respect to the quality of the sample and the presence and localization of the myenteric plexus. High-resolution scans revealed details of the myenteric plexus, including the ganglia, interganglionic nerve fascicles, and surrounding tissue.

### Normal structure of the ileal myenteric plexus

**Ganglion:** The shape of the ganglia was uneven toward both the muscle layers and interganglionic nerve fascicles. The smaller or larger irregularities contained one or more neurons and glial cells (Figures 1, 2A, 4A-D, and 5).

In the surface view of the ganglia, a parallel arrangement of telocytes with long thin “primary” telopodes originating directly from the cellular bodies could be observed, from which shorter “secondary” telopodes radiated sidewise, building up a network (Figures 1A-C, 3B, 4A and B). Occasionally, at the optimal transverse view of the ganglion, a double layer of thin cytoplasmic projections was present (Figure 2B), corresponding to the immunohistochemical demonstration of telocytes and ICCs[17].

Both larger and smaller neurons had mostly rounded nuclei and nucleoli, where larger neurons had finely granulated cytoplasm with a paler network between the granules, whereas the smaller neurons had slightly denser and more homogeneous cytoplasm (Figures 2B and 3B-D). Axons were occasionally observed (Figure 2A). Small glial cells were present around and between the neurons (Figures 2A, 3C and D). No degenerating neurons were found in either of the two younger individuals. In the 82-year-old control, however, one neuron with a shrunken, dark body, pyknotic small almost black nucleus and larger autophagic vacuoles could be observed in addition to numerous normal neurons (not shown).

### Nerve fascicles and spindle-shaped cell layer

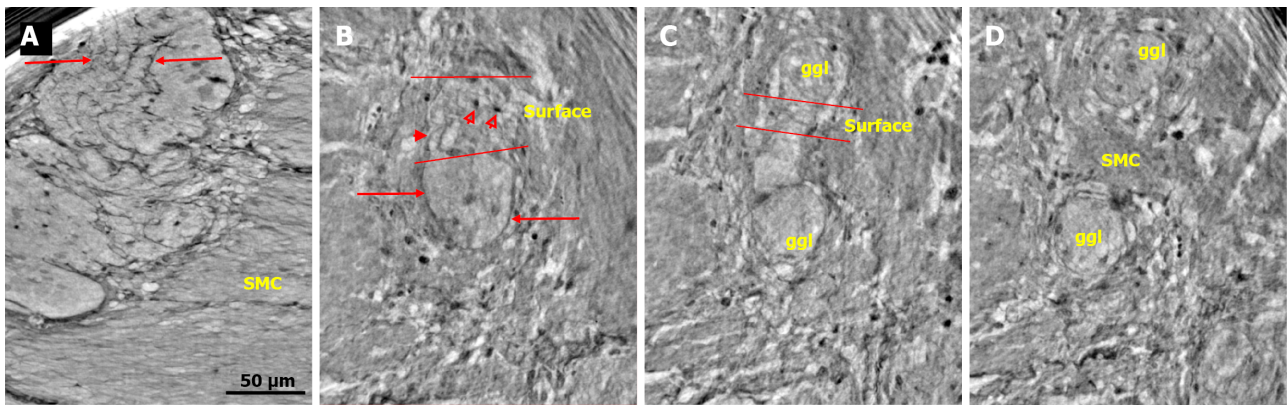
The nerve fascicles had normal architecture. Parallel thin telopodes separated the individual axons (Figures 2C and 3A-C). Some spindle-shaped cells had very thin, dark nuclei, whereas the nuclei of others were larger and cigar-like.

### Pathological findings of the ileal myenteric plexus

Four patients had lymphocytic ganglioneuritis or lymphocytic neuritis, and two patients had only visceral degenerative neuropathy. No alterations were observed in the general architecture of the myenteric ganglia. Nevertheless, several pathological changes could be observed, partly corresponding to the light microscopic findings, as shown in the insets of the figures. Cellular changes occurred in all six patients with dysmotility. Suspected lymphocytes were found within the ganglion only in one patient. The lack of lymphocytic attack on the ganglion in other patients can be explained by the focal nature of inflammation.

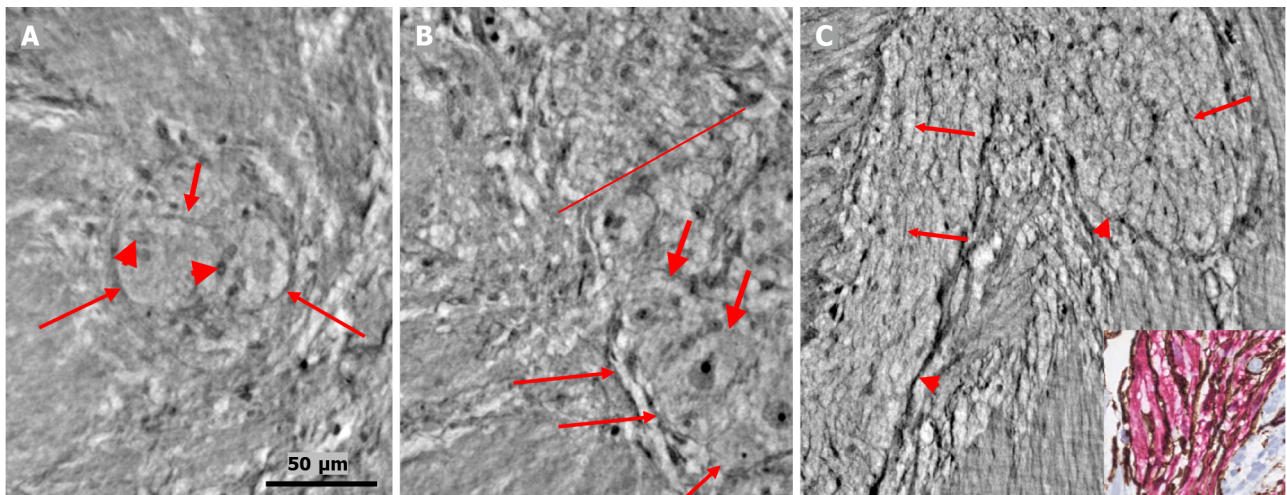
### Pathological neuronal changes

The cytoplasm of several neurons contained vacuoles. Many of the vacuoles contained small dark granules (Figure 5A, C, and D) (autophagic vacuoles/Lipofuscin; 5D-inset: PAS-D<sup>+</sup>). In one patient, several neurons exhibited pale cytoplasm (Figure 4A-D) (chromatolysis), and a large homogeneous irregular dark area was present (Figure 4F) (4F-inset: Sequestosome p62<sup>+</sup>). Apoptotic shrunken neurons had compact, dark cytoplasm with small, irregular, pyknotic nuclei (Figures 4C-E, 5B and 6) (4E-inset H&E; 5B-inset: Apoptosis H&E). These neurons were observed in three patients at the ganglion border without telopodes in a few virtual slices (Figure 4B-D), possibly representing the ejection of a dead neuron (Figures 4B-D and 6). Very dense dark inclusions with similar substructures were found in two patients, which are foreign structures for the normal ganglion; one of these bodies is shown in serial virtual slices (Figure 4A-C) (4A-C: Hyaline bodies; 4A and B-insets: PAS-D<sup>+</sup>). At 6.8 μm in Figure 4A, an inner structure with a central pale area surrounded by an irregular dark ring can be seen within the body (Figure 4B). When viewing 4.0 μm deeper, there is a semi-dense “half-moon” at the edge of the hyaline body (Figure 4C).



DOI: 10.3748/wjg.v28.i29.3994 Copyright ©The Author(s) 2022.

**Figure 1 Ganglion from healthy human ileum.** A: Part of the myenteric ganglion in two portions. Quite regular, almost parallel, thin cytoplasmic projections of telocytes (telopodes) with short, thin "spines" on the surface are observed (between arrows). The scale bar (50 µm) was applied to all subfigures; B: A small portion of the ganglion containing two neurons. On the surface of the ganglion (between the two lines), the cellular nuclei of the two telocytes were observed as dark spots (empty arrowheads). Telopodes radiate from their body. Arrows indicate the telopodes around the ganglion. A telopode can be followed toward the surface (arrowhead); C: 16.9 µm deeper from Figure B, two portions appeared with thin telopodes on the surface; D: 10.1 µm deeper from Figure C, SMCs are observed between the two portions. B-D are representative virtual slices from a series covering 27.0 µm thickness of the ganglion. Ggl: Ganglion; SMC: Smooth muscle cells.



DOI: 10.3748/wjg.v28.i29.3994 Copyright ©The Author(s) 2022.

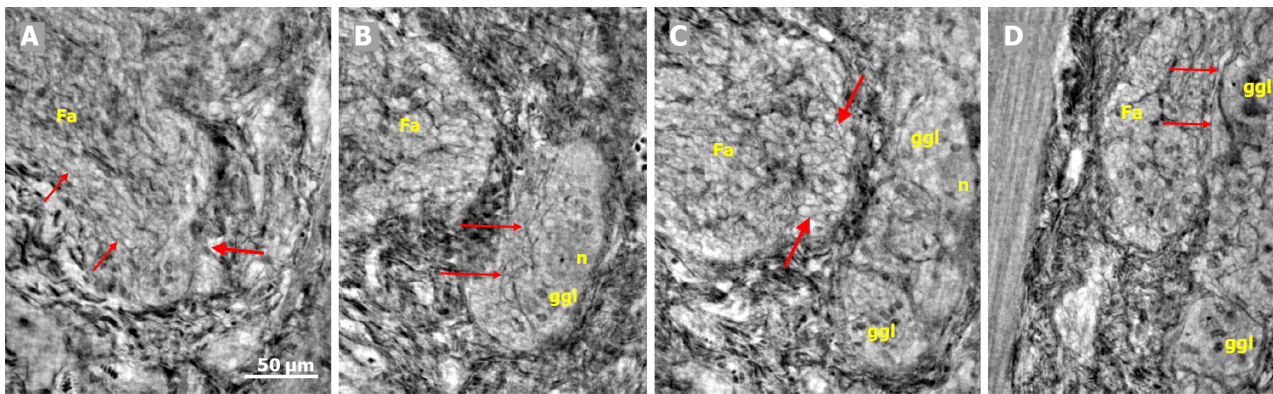
**Figure 2 Ganglion and fascicle from healthy human ileum.** A: Within a portion of the ganglion, there is a neuron with an axon (thick arrow). Arrowheads indicate glial cells. Thin arrows indicate a single layer of telopodes at the border of the ganglion. The scale bar (50 µm) was applied to all subfigures; B: Part of a ganglion with several large (thick arrows) and medium-large (short thin arrow) neurons. The nuclei contain dark nucleoli. The cytoplasm is slightly granulated. Above the straight line, a small area of the neuropil was observed. Long thin arrows indicate the double-cell layer at the border; C: Normal nerve fascicle and thicker nerve with telopodes separating axons (arrows). Note the single layer of telopodes around the fascicle and nerve (arrowheads). Inset: Normal nerve fascicles stained with double immunohistochemistry. Telocytes run parallel to Schwann cells (light microscopy; S100: Schwann cells red; CD34: Telocytes brown).

### Pathological change of the nerve fascicles and periganglionic spindle-shaped cell layer

In one patient who was diagnosed with lymphocytic ganglioneuritis, a segment of the periganglionic spindle-shaped cell layer showed vacuolization and/or was absent within a 19.9 µm distance along the length axis of the bowel sample (Figure 5). The largest window in this absence was 16.1 µm in the virtual slices (Figure 5B). At a 7.8 µm deeper level (Figure 5C), a double layer of thin cellular projections appeared at the border of the defect, whereas at an additionally 4.7 µm deeper, one intact layer of cellular projections was again present between the ganglion and the surrounding tissue (Figure 5D).

### Video-film

In the video film from one patient, more than one dozen neurons and glial cells could be observed (Supplementary material). Almost all the neurons showed various types of degeneration. Furthermore, one pre-apoptotic neuron in the lower part of the ganglion was probably in contact with the tip of the incomplete septum, and hence, extended into the surrounding tissue (Supplementary material).



DOI: 10.3748/wjg.v28.i29.3994 Copyright ©The Author(s) 2022.

**Figure 3** Series of virtual slices covering 113.6  $\mu\text{m}$  thickness at the border between the nerve fascicle and the ganglion. A: Thick fascicle with parallel telopodes (thin arrows). There is a small peripheral part of the ganglion (thick arrow); B: 62.2  $\mu\text{m}$  deeper from Figure A. Connective tissue cells between the fascicle and the superficial part of the ganglion. Normal large neurons and nuclei of several glial cells in the ganglion. A network of telopodes is present on the surface of the ganglion (arrows); C: 11.5  $\mu\text{m}$  deeper from Figure B. The thickness of the connective tissue is diminished between the fascicle and the periphery of the ganglion, with two neurons and small glial cells. Transversally cut vesicle-like axons (between the arrows) on the right end of the fascicle; D: 39.9  $\mu\text{m}$  deeper from Figure C, the fascicle and ganglion are united. Thin arrows show telopodes. The scale bar (50  $\mu\text{m}$ ) applies to all the subfigures. Fa: Fascicle; ggl: Ganglion; n: Neuron.

## DISCUSSION

The main qualitative finding in the present study was that X-ray phase-contrast nanotomography could analyze the different cellular components of the myenteric plexus in more than 6000 serial virtual slices, which could reveal minor changes not seen under the light microscope. We could image large volumes with finer sampling resolution with shorter distances between sections along the sample direction, that is, below the standard thickness of a histological scan.

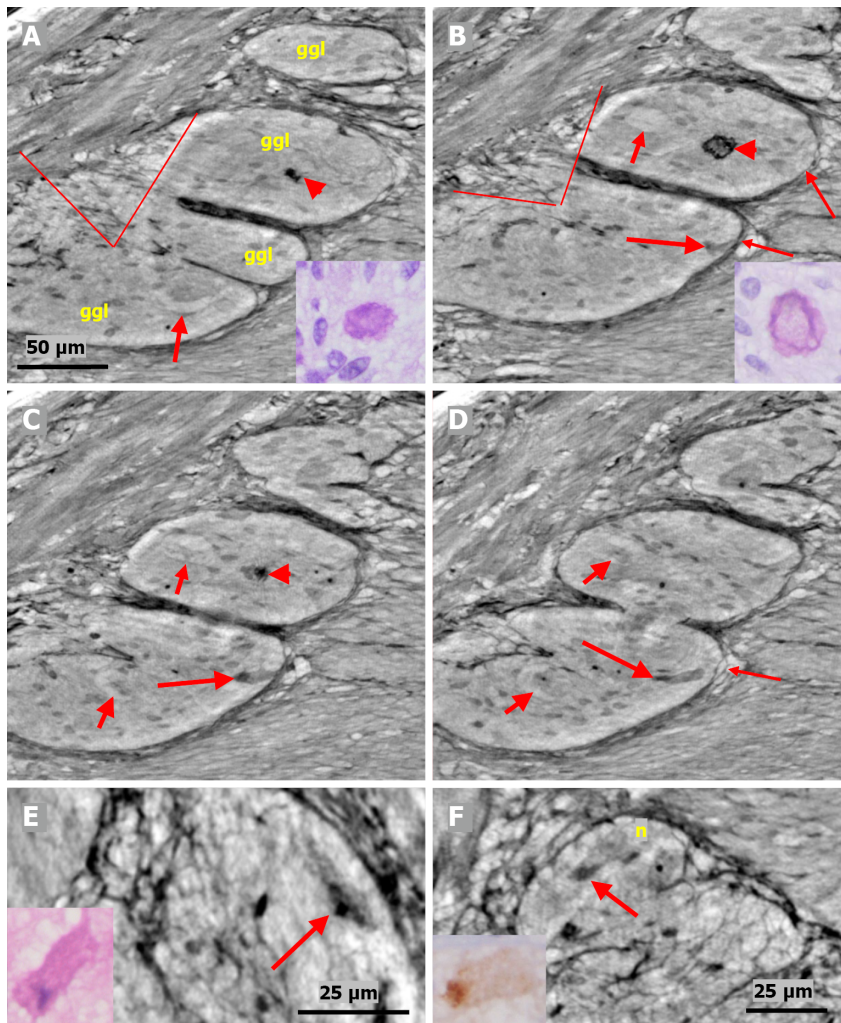
A study of the normal ganglia revealed that their shape is not usually seen in the transverse sections under a light microscope with a well-defined border. In serial virtual slices, the ganglia have smaller or larger irregularities, with one or a few neurons and glial cells protruding into the muscle layers or the intermyenteric connective tissue. Within the ganglia, neurons of various sizes and glial cells could be clearly differentiated. The absence of thin cytoplasmic projections in the neuropil corroborates our previous finding in the ileal ganglia, namely the lack of telopodes in the ileum in contrast to the colon [17]. The presence of one degenerating neuron in the 82-year-old control may be the result of aging starting at around 40-50 years of age [18].

The optimal transverse sections showed two clear layers of cellular projections surrounding the ganglion, in accordance with our previous immunohistochemical findings [17]. The inner layer consisted of cytoplasmic projections of telocytes called telopodes, which were situated almost parallel to each other, in agreement with immunohistochemical observations [17]. The outer layer is composed of an ICC [17].

Pathological changes from the patients revealed different types of neuronal degeneration (vacuolization, autophagic vacuoles/Lipofuscin, chromatolysis, and apoptosis) and the presence of a hyaline body within the ganglion, as observed under a light microscope by the golden standard of various staining techniques [8]. Furthermore, p62+ sequestosomes were also observed in accordance with the findings of Alafuzoff *et al* [19].

Three new phenomena were discovered with the present phase-contrast nanotomography, which cannot be observed under a light microscope because of the thickness of the paraffin sections. First, the presence of a semi-dense “half-moon” attached to the hyaline body could hypothetically be one of the end stages of cellular death. Second, the phenomenon of a probable expulsion of dead neurons could be followed in the virtual serial slices because of the occurrence of a short “opening” of the telopode-layer between the surrounding connective tissue and shrunken apoptotic neurons. Third, the total absence of the single telopode layer within the 16.1  $\mu\text{m}$  “window” could possibly have negatively affected the stability of the ganglion.

The virtual histology of the myenteric ganglion using X-ray nanotomography has advantages, disadvantages, and future possibilities. The main advantage is that the method can exactly measure the volumes of chosen tissue components following segmentation, as have been previously published [5]. The second advantage is the possibility to analyze several hundred serial virtual slices at subcellular, isotropic resolution, and through this, discover “nano-changes” which cannot be seen using the light microscope. Because the neuron size is 15-40  $\mu\text{m}$ , the ENS is difficult to examine in conventional histological sections of 3-5  $\mu\text{m}$ . Slow videos make it possible to follow the relationships between the various tissue components. The third advantage is the flexibility in sample preparation; samples can be examined with or without paraffin embedding (*e.g.*, in liquid or epoxy resin) or staining. Thus, the

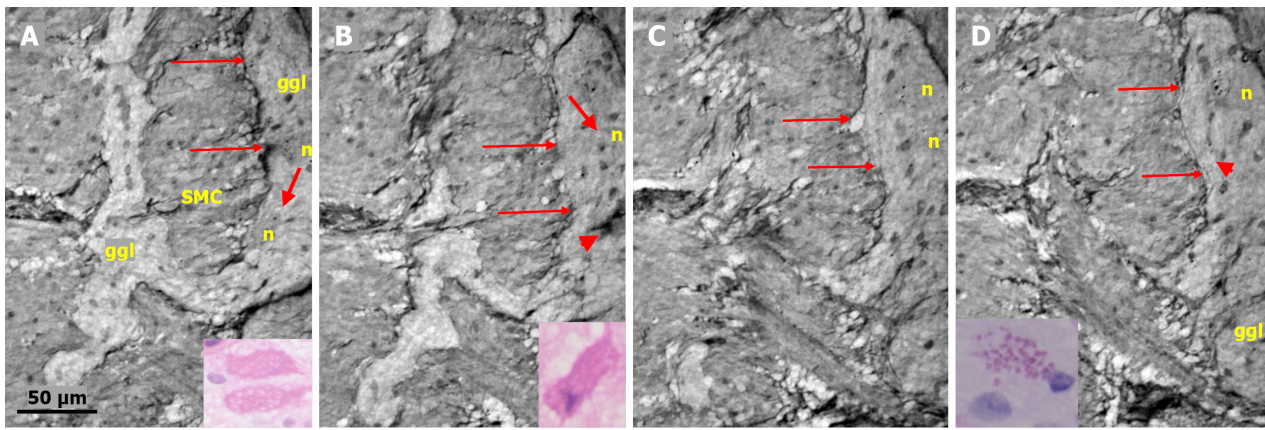


DOI: 10.3748/wjg.v28.i29.3994 Copyright ©The Author(s) 2022.

**Figure 4** Series of virtual slices covering 17.2  $\mu\text{m}$  thickness of the ganglion from one patient. A: Four portions of the ganglion. There is a dark body at the center of one of these areas (arrowheads). An arrow indicates a neuron with a very pale homogeneous cytoplasm below the nucleus. Between the straight lines, a network of telopodes is observed on the ganglion surface. Incomplete septa between portions. Scale bar (50  $\mu\text{m}$ ) is applied to subfigures A-D. Inset: Hyaline body in the ganglion [1<sup>st</sup> level of serial sections; light microscopy; periodic acid-Schiff with diastase (PAS-D) staining]; B: 6.8  $\mu\text{m}$  from Figure A., three portions of the ganglia are completely separated, and the surface area is smaller (between straight lines). The central dark body shows an irregular dense outer layer and central light area (arrowhead). A new neuron with pale cytoplasm is seen in the middle portion (short arrow). Intact telopodes form the border between the ganglion and the periganglionic connective tissue rim (thin arrows). An almost triangle-shaped moderately dense area is seen below the telopode corresponding to an apoptotic neuron (long arrow; see also C and D). Inset: The central region of the hyaline body is negative, whereas the outer layer is positive with PAS-D staining (2<sup>nd</sup> level of serial sections, light microscopy; PAS-D); C: 4.0  $\mu\text{m}$  from Figure B. The hyaline body is without a central pale area (arrowhead), with a semi-dense irregular half-moon to the left. The two neurons had a pale cytoplasm (short arrows). A dark pyknotic nucleus appeared in the semi-dense cytoplasm at the border showing an apoptotic neuron corresponding to the "dark triangle" in Figure B (long arrow); D: 6.4  $\mu\text{m}$  deeper from Figure C. Two of the portions are united. Nuclei are present in neurons with pale cytoplasm (short arrows). Intact telopodes are present between the degenerated apoptotic cells (long arrow) and the periganglionic space (thin arrow); E: Digital magnification of a shrunken neuron with a darker cytoplasm, small vacuoles, and enlarged nucleolus. Scale bar: 25  $\mu\text{m}$  Inset: Pre-apoptotic neurons with pyknotic nucleus and vacuole-containing amphophilic cytoplasm (light microscopy; H&E staining); F: There is a homogeneous circumscribed "inclusion" in the neuron, suggesting a sequestosome, as seen in the inset (arrow). Scale bar: 25  $\mu\text{m}$ . Inset: Large p62<sup>+</sup> aggregates in neurons (arrow; light microscopy; p62 immunohistochemistry). Scale bars of 50 or 25  $\mu\text{m}$  included. Ggl: Ganglion; n: Neuron; PAS-D: Periodic acid-schiff with diastase.

samples require less handling and fewer preparation steps[20].

The current established method to diagnose enteric neuropathy uses immunohistochemistry with a wide range of staining according to a standardized protocol[8,21]. The strength of this method lies in the exact identification of different cell types and tissue structures. The weakness is that there is a wide range of different molecules and structures that can vary in abundance among different patients with the same diagnosis. We do not know whether these changes are causal or primary, or whether they are secondary or compensatory. Due to the large variation between patients, no uniform pattern has been determined for the diagnosis of enteric neuropathy, and thus, some of the information did not add substantial value to the examination. The current description of neurons, glial cells, and spindle-shaped cells appears to be sufficient for diagnosis.



DOI: 10.3748/wjg.v28.i29.3994 Copyright ©The Author(s) 2022.

**Figure 5** Series of virtual slices covering 19.9  $\mu\text{m}$  thickness of the ganglion from one patient. A: Two portions of the ganglion with smooth muscle cells between them. Long arrows indicate the continuous layer of telopodes with tiny vesicles bordering the ganglion. A string of glial cell nuclei was present within the left portion. The thick arrow shows the vacuole above the nucleus of the neuron. Four small dark granules were present in the other neurons. Inset: Several vacuoles fill the cytoplasm of the two degenerating neurons (light microscopy and H&E staining); B: 7.4  $\mu\text{m}$  deeper from Figure A. Between the thin arrows there is no continuous layer of telopodes, instead some vesicles are seen. The left portion has disappeared. The remaining portion is part of a pre-apoptotic neuron with a dark cytoplasm and pyknotic nucleus (arrowhead). Above this neuron is the nuclei of normal glial cells. The thick arrow indicates a vacuole in the neuron. Inset: Apoptotic neurons with strongly amphophilic cytoplasm and rest of the pyknotic nuclei (light microscopy; H&E staining); C: 7.8  $\mu\text{m}$  deeper from Figure B. The defect of the telopodes (between the thin arrows) was shorter. Double layer of telopodes below the defect. In the upper part of the ganglion, there is a large neuron with a few small dark, dense dots, whereas the pre-apoptotic neuron from the middle of the ganglion is no longer present; D: 4.7  $\mu\text{m}$  deeper from Figure C. There is a continuous layer of telopodes (between arrows) with a "remnant" of the double layer, as shown in Figure C. The dark granules in the neurons were larger and more numerous. Arrowhead shows a neuron with both dark granules and vacuoles. Inset: The cytoplasm of the neurons was filled with diastase-resistant PAS+ lipofuscin granules (light microscopy; PAS-D staining). The scale bar (50  $\mu\text{m}$ ) applies to all the subfigures. Ggl: Ganglion; H&E: Hematoxylin & eosin; n: Neuron; PAS: Periodic acid-Schiff; PAS-D: Periodic acid-Schiff with diastase; SMC: Smooth muscle cells.

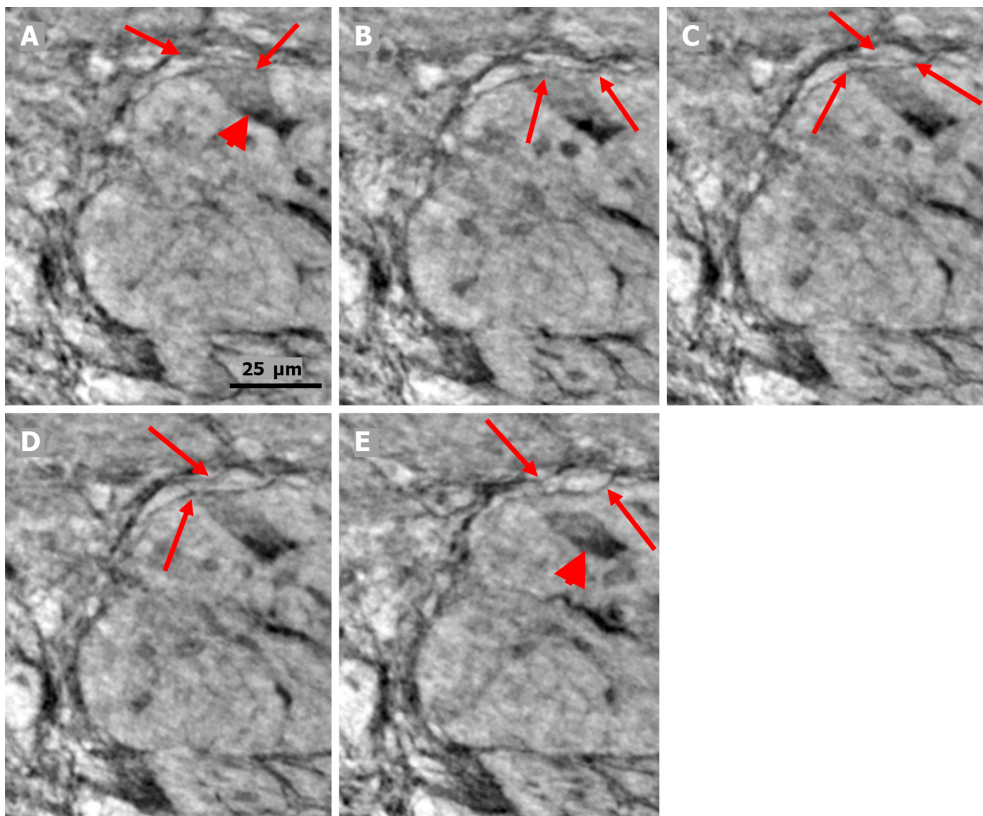
Fluorescence confocal microscopy has been performed with serial sectioning to mimic three-dimensional (3D) imaging; however, the maximal thickness of viewing is still limited, and the space between sections is larger[22-25]. Recently, another method using immunohistochemistry and confocal microscopy was developed for the quantitative analysis of full-thickness bowel biopsies[26]. These different efforts to improve the analysis of ENS prove the importance of clinicians obtaining more information about the function and dysfunction of the gastrointestinal tract.

Among the disadvantages were the limited access to synchrotron beamtime and the cost of the entire process in terms of money and manpower. Furthermore, because the ganglia of the ENS are very sparse, especially in patients with dysmotility, and the myenteric plexus can fold and curve beneath what is visible on the surface of the block, it is very difficult to correctly punch the tissue of interest based on a histological section. Hence, multi-scale X-ray phase-contrast tomography, which involves scanning a tissue block with a mm-sized field-of-view at  $\mu\text{m}$ -resolution and then imaging specific features of interest in greater detail using local nanotomography on the full block (instead of extracting biopsy punches as in this work), would be preferable and has been proven to be feasible at different synchrotron beamlines, such as TOMCAT[27,28] and P10/GINIX[29-31].

In the future, the combination of immunohistochemistry with X-ray phase-contrast nanotomography, such as immuno-electron microscopy[32], or with joint X-ray phase-contrast tomography and focused ion beam scanning electron microscopy (FIB-SEM) could provide unique possibilities to study targeted cells and their internal and external relationships[33]. In addition, this technique can determine the exact volume of the target tissue components[5].

## CONCLUSION

Virtual sectioning by X-ray phase-contrast nanotomography is a method that provides a unique analysis of the myenteric ganglion, revealing minor pathological changes that cannot be discovered using light microscopy or other two-dimensional scanning methods to study the relationship between various tissue components.



DOI: 10.3748/wjg.v28.i29.3994 Copyright ©The Author(s) 2022.

**Figure 6** Series of virtual slices covering 6.4  $\mu\text{m}$  thickness of the ganglion from one patient. A: Neuron with shrunken pyknotic nucleus and dark cytoplasm containing vacuoles at the edge of the ganglion (arrowhead). A part of the cytoplasm of the pre-apoptotic neuron is present between the telopodes (arrows); B: 2.0  $\mu\text{m}$  deeper from Figure A. The lower telopode was discontinuous (arrows); C: 0.7  $\mu\text{m}$  deeper from Figure B. The two telopodes are intact, and almost all of the cytoplasm between them has disappeared; D: 0.7  $\mu\text{m}$  deeper from Figure C. Pre-apoptotic neurons seem to be in contact with the lower telopode; E: 3.0  $\mu\text{m}$  deeper from Figure D. The pre-apoptotic neuron (arrowhead) lies within the ganglion, without contact with the telopodes. Arrows point to two telopodes on the figures. The scale bar (25  $\mu\text{m}$ ) applies to all the subfigures.

## ARTICLE HIGHLIGHTS

### Research background

The enteric nervous system (ENS) is difficult to study because of its deep localization in the intestinal wall. The limited sections visualized by light microscopy cannot show the size of the neurons or the interconnection between different parts of the ENS or different cell types.

### Research motivation

Since the ENS is difficult to examine, patients with gastrointestinal dysmotility are not properly examined, diagnosed, and treated. They can experience symptoms for several years before a proper diagnosis is established.

### Research objectives

The main objective of this study was to examine whether X-ray phase-contrast tomography could improve the visualization of the ENS. We realized that the ENS could be visualized without any prior staining, and the information provided was superior to conventional light microscopy in some respects. Thus, this method should be further evaluated in future studies.

### Research methods

Full-thickness biopsies from the ileum of patients with dysmotility and controls were examined using X-ray phase-contrast tomography. For comparison, the same samples were examined using immunohistochemistry. This is the first time that bowel biopsies have been examined using X-ray tomography, and the histopathology has been described in detail.

### Research results

This study showed that X-ray phase-contrast tomography can be used to study the ENS in detail to describe normal and pathological cells and tissue structures. The interconnections between the cells and

structures can be visualized. Some new findings could not have been observed using conventional light microscopy.

### **Research conclusions**

Virtual sectioning by X-ray phase-contrast nanotomography provides a unique analysis of the myenteric ganglion, revealing minor pathological changes that cannot be discovered by light microscopy, to follow the relationship between various tissue components.

### **Research perspectives**

This method needs to be further studied in larger cohorts, with scanning of whole paraffin blocks combined with different staining methods to try to improve the identification of different cell types and tissue structures. More healthy controls should be examined to obtain reference values for health and disease.

---

## **ACKNOWLEDGEMENTS**

The authors thank Maria Teresa Moreira Jara and Maria Nilsson for their technical assistance and the pathologists for control sample collection. The valuable discussion with Anca Dragomir, MD, PhD, Uppsala University, regarding possible artifacts, is greatly appreciated.

---

## **FOOTNOTES**

**Author contributions:** Veress B performed the histochemical and pathological analyses of the X-ray data and wrote the initial draft together with Ohlsson B; Peruzzi N, Eckermann M, and Frohn J scanned the samples; Peruzzi N analyzed the technical data; all authors planned and designed the study, contributed to intellectual analysis of the results, and approved the final version of the manuscript.

**Supported by** the Development Foundation of Region Skåne, No. REGSKANE-818781 and No. 2018-Projekt0024; and the Foundation Skåne University Hospital, No. 2020-0000028.

**Institutional review board statement:** The study was reviewed and approved by the Regional Ethics Review Board at Lund University (2009/209, Date of approval 28/04/2009; 2012/527, Date of approval 16/10/2012 and 2018/132, Date of approval 02/08/2018) and the Swedish Biobank Act.

**Informed consent statement:** All study participants provided informed written consent prior to study enrollment.

**Conflict-of-interest statement:** There are no conflicts of interest to report.

**Data sharing statement:** No additional data is available.

**STROBE statement:** The authors have read the STROBE Statement – checklist of items, and the manuscript was prepared and revised according to the STROBE Statement – checklist of items.

**Open-Access:** This article is an open-access article that was selected by an in-house editor and fully peer-reviewed by external reviewers. It is distributed in accordance with the Creative Commons Attribution NonCommercial (CC BY-NC 4.0) license, which permits others to distribute, remix, adapt, build upon this work non-commercially, and license their derivative works on different terms, provided the original work is properly cited and the use is non-commercial. See: <https://creativecommons.org/licenses/by-nc/4.0/>

**Country/Territory of origin:** Sweden

**ORCID number:** Bela Veress 0000-0001-9529-6809; Niccolò Peruzzi 0000-0002-2929-4247; Marina Eckermann 0000-0001-6418-4310; Jasper Frohn 0000-0003-3849-6032; Tim Salditt 0000-0003-4636-0813; Bodil Ohlsson 0000-0002-9142-5244.

**Corresponding Author's Membership in Professional Societies:** UEG; Swedish Society of Gastroenterology.

**S-Editor:** Chen YL

**L-Editor:** A

**P-Editor:** Chen YL

## REFERENCES

- 1 **Furness JB**, Callaghan BP, Rivera LR, Cho HJ. The enteric nervous system and gastrointestinal innervation: integrated local and central control. *Adv Exp Med Biol* 2014; **817**: 39-71 [PMID: [24997029](#) DOI: [10.1007/978-1-4939-0897-4\\_3](#)]
- 2 **Wingate D**, Hongo M, Kellow J, Lindberg G, Smout A. Disorders of gastrointestinal motility: towards a new classification. *J Gastroenterol Hepatol* 2002; **17** Suppl: S1-14 [PMID: [12000590](#) DOI: [10.1046/j.1440-1746.17.s1.7.x](#)]
- 3 **Keller J**, Bassotti G, Clarke J, Dinning P, Fox M, Grover M, Hellström PM, Ke M, Layer P, Malagelada C, Parkman HP, Scott SM, Tack J, Simren M, Törnblom H, Camilleri M; International Working Group for Disorders of Gastrointestinal Motility and Function. Expert consensus document: Advances in the diagnosis and classification of gastric and intestinal motility disorders. *Nat Rev Gastroenterol Hepatol* 2018; **15**: 291-308 [PMID: [29622808](#) DOI: [10.1038/nrgastro.2018.7](#)]
- 4 **Hammar O**, Ohlsson B, Veress B, Alm R, Fredrikson GN, Montgomery A. Depletion of enteric gonadotropin-releasing hormone is found in a few patients suffering from severe gastrointestinal dysmotility. *Scand J Gastroenterol* 2012; **47**: 1165-1173 [PMID: [22835010](#) DOI: [10.3109/00365521.2012.706826](#)]
- 5 **Peruzzi N**, Veress B, Dahlin LB, Salditt T, Andersson M, Eckermann M, Frohn J, Robisch AL, Bech M, Ohlsson B. 3D analysis of the myenteric plexus of the human bowel by X-ray phase-contrast tomography - a future method? *Scand J Gastroenterol* 2020; **55**: 1261-1267 [PMID: [32907418](#) DOI: [10.1080/00365521.2020.1815079](#)]
- 6 **Eckermann M**, Peruzzi N, Frohn J, Bech M, Englund E, Veress B, Salditt T, Dahlin LB, Ohlsson B. 3d phase-contrast nanotomography of unstained human skin biopsies may identify morphological differences in the dermis and epidermis between subjects. *Skin Res Technol* 2021; **27**: 316-323 [PMID: [33022848](#) DOI: [10.1111/srt.12974](#)]
- 7 **Törnblom H**, Lindberg G, Nyberg B, Veress B. Full-thickness biopsy of the jejunum reveals inflammation and enteric neuropathy in irritable bowel syndrome. *Gastroenterology* 2002; **123**: 1972-1979 [PMID: [12454854](#) DOI: [10.1053/gast.2002.37059](#)]
- 8 **Lindberg G**, Törnblom H, Iwarzon M, Nyberg B, Martin JE, Veress B. Full-thickness biopsy findings in chronic intestinal pseudo-obstruction and enteric dysmotility. *Gut* 2009; **58**: 1084-1090 [PMID: [19136514](#) DOI: [10.1136/gut.2008.148296](#)]
- 9 **Knowles CH**, Veress B, Kapur RP, Wedel T, Farrugia G, Vanderwinden JM, Geboes K, Smith VV, Martin JE, Lindberg G, Milla PJ, De Giorgio R. Quantitation of cellular components of the enteric nervous system in the normal human gastrointestinal tract--report on behalf of the Gastro 2009 International Working Group. *Neurogastroenterol Motil* 2011; **23**: 115-124 [PMID: [21175997](#) DOI: [10.1111/j.1365-2982.2010.01657.x](#)]
- 10 **Knowles CH**, De Giorgio R, Kapur RP, Bruder E, Farrugia G, Geboes K, Lindberg G, Martin JE, Meier-Ruge WA, Milla PJ, Smith VV, Vanderwinden JM, Veress B, Wedel T. The London Classification of gastrointestinal neuromuscular pathology: report on behalf of the Gastro 2009 International Working Group. *Gut* 2010; **59**: 882-887 [PMID: [20581236](#) DOI: [10.1136/gut.2009.200444](#)]
- 11 **Töpperwien M**, van der Meer F, Stadelmann C, Salditt T. Three-dimensional virtual histology of human cerebellum by X-ray phase-contrast tomography. *Proc Natl Acad Sci U S A* 2018; **115**: 6940-6945 [PMID: [29915047](#) DOI: [10.1073/pnas.1801678115](#)]
- 12 **Salditt T**, Osterhoff M, Krenkel M, Wilke RN, Priebe M, Bartels M, Kalbfleisch S, Sprung M. Compound focusing mirror and X-ray waveguide optics for coherent imaging and nano-diffraction. *J Synchrotron Radiat* 2015; **22**: 867-878 [PMID: [26134789](#) DOI: [10.1107/S1600577515007742](#)]
- 13 **Cloetens P**, Ludwig W, Baruchel J, Van Dyck D, Landuyt JV, Guigay JP, Schlenker M. Holotomography: Quantitative phase tomography with micrometer resolution using hard synchrotron radiation x rays. *Appl Phys Lett* 1999; **75**: 2912 [DOI: [10.1063/1.125225](#)]
- 14 **Groso A**, Stampanoni M, Abela R, Schneider P, Linga S, Müller R. Phase contrast tomography: An alternative approach. *Appl Phys Lett* 2006; **88**: 214104 [DOI: [10.1063/1.2207221](#)]
- 15 **De Witte Y**, Boone M, Vlassenbroeck J, Dierick M, Van Hoorebeke L. Bronnikov-aided correction for x-ray computed tomography. *J Opt Soc Am A Opt Image Sci Vis* 2009; **26**: 890-894 [PMID: [19340263](#) DOI: [10.1364/josaa.26.000890](#)]
- 16 **Lohse LM**, Robisch AL, Töpperwien M, Marezke S, Krenkel M, Hagemann J, Salditt T. A phase-retrieval toolbox for X-ray holography and tomography. *J Synchrotron Radiat* 2020; **27**: 852-859 [PMID: [32381790](#) DOI: [10.1107/S1600577520002398](#)]
- 17 **Veress B**, Ohlsson B. Spatial relationship between telocytes, interstitial cells of Cajal and the enteric nervous system in the human ileum and colon. *J Cell Mol Med* 2020; **24**: 3399-3406 [PMID: [31983076](#) DOI: [10.1111/jcmm.15013](#)]
- 18 **Hanewinkel R**, Drenthen J, van Oijen M, Hofman A, van Doorn PA, Ikram MA. Prevalence of polyneuropathy in the general middle-aged and elderly population. *Neurology* 2016; **87**: 1892-1898 [PMID: [27683845](#) DOI: [10.1212/WNL.0000000000003293](#)]
- 19 **Alafuzoff I**, Popova SN, Veress B. Neuronal protein alteration in enteric dysmotility syndrome. *J Alzheimers Dis Parkinsonism* 2016; **6**: 212-216 [DOI: [10.4172/2161-0460.1000212](#)]
- 20 **Eckermann M**, van der Meer F, Cloetens P, Ruhwedel T, Möbius W, Stadelmann C, Salditt T. Three-dimensional virtual histology of the cerebral cortex based on phase-contrast X-ray tomography. *Biomed Opt Express* 2021; **12**: 7582-7598 [PMID: [35003854](#) DOI: [10.1364/BOE.434885](#)]
- 21 **Lehtonen HJ**, Sipponen T, Tojkander S, Karikoski R, Järvinen H, Laing NG, Lappalainen P, Aaltonen LA, Tuupainen S. Segregation of a missense variant in enteric smooth muscle actin  $\gamma$ -2 with autosomal dominant familial visceral myopathy. *Gastroenterology* 2012; **143**: 1482-1491.e3 [PMID: [22960657](#) DOI: [10.1053/j.gastro.2012.08.045](#)]
- 22 **Vanderwinden JM**, Rumessen JJ, De Laet MH, Vanderhaeghen JJ, Schiffmann SN. CD34+ cells in human intestine are fibroblasts adjacent to, but distinct from, interstitial cells of Cajal. *Lab Invest* 1999; **79**: 59-65 [PMID: [9952111](#)]
- 23 **Toma H**, Nakamura K, Kuraoka A, Tanaka M, Kawabuchi M. Three-dimensional structures of c-Kit-positive cellular networks in the guinea pig small intestine and colon. *Cell Tissue Res* 1999; **295**: 425-436 [PMID: [10022963](#) DOI: [10.1007/s004410051249](#)]
- 24 **Cobine CA**, Hennig GW, Kurahashi M, Sanders KM, Ward SM, Keef KD. Relationship between interstitial cells of Cajal, fibroblast-like cells and inhibitory motor nerves in the internal anal sphincter. *Cell Tissue Res* 2011; **344**: 17-30 [PMID: [21337122](#) DOI: [10.1007/s00441-011-1138-1](#)]

- 25 **Grover M**, Bernard CE, Pasricha PJ, Parkman HP, Abell TL, Nguyen LA, Snape W, Shen KR, Sarr M, Swain J, Kendrick M, Gibbons S, Ordog T, Farrugia G. Platelet-derived growth factor receptor  $\alpha$  (PDGFR $\alpha$ )-expressing "fibroblast-like cells" in diabetic and idiopathic gastroparesis of humans. *Neurogastroenterol Motil* 2012; **24**: 844-852 [PMID: 22650155 DOI: 10.1111/j.1365-2982.2012.01944.x]
- 26 **Graham KD**, López SH, Sengupta R, Shenoy A, Schneider S, Wright CM, Feldman M, Furth E, Valdivieso F, Lemke A, Wilkins BJ, Naji A, Doolin EJ, Howard MJ, Heuckeroth RO. Robust, 3-Dimensional Visualization of Human Colon Enteric Nervous System Without Tissue Sectioning. *Gastroenterology* 2020; **158**: 2221-2235.e5 [PMID: 32113825 DOI: 10.1053/j.gastro.2020.02.035]
- 27 **Norvik C**, Westöö CK, Peruzzi N, Lovric G, van der Have O, Mokso R, Jeremiasen I, Brunnström H, Galambos C, Bech M, Tran-Lundmark K. Synchrotron-based phase-contrast micro-CT as a tool for understanding pulmonary vascular pathobiology and the 3-D microanatomy of alveolar capillary dysplasia. *Am J Physiol Lung Cell Mol Physiol* 2020; **318**: L65-L75 [PMID: 31596108 DOI: 10.1152/ajplung.00103.2019]
- 28 **Westöö C**, Norvik C, Peruzzi N, van der Have O, Lovric G, Jeremiasen I, Tran PK, Mokso R, de Jesus Perez V, Brunnström H, Bech M, Galambos C, Tran-Lundmark K. Distinct types of plexiform lesions identified by synchrotron-based phase-contrast micro-CT. *Am J Physiol Lung Cell Mol Physiol* 2021; **321**: L17-L28 [PMID: 33881927 DOI: 10.1152/ajplung.00432.2020]
- 29 **Frohn J**, Pinkert-Leetsch D, Missbach-Güntner J, Reichardt M, Osterhoff M, Alves F, Salditt T. 3D virtual histology of human pancreatic tissue by multiscale phase-contrast X-ray tomography. *J Synchrotron Radiat* 2020; **27**: 1707-1719 [PMID: 33147198 DOI: 10.1107/S1600577520011327]
- 30 **Reichardt M**, Frohn J, Khan A, Alves F, Salditt T. Multi-scale X-ray phase-contrast tomography of murine heart tissue. *Biomed Opt Express* 2020; **11**: 2633-2651 [PMID: 32499949 DOI: 10.1364/BOE.386576]
- 31 **Eckermann M**, Schmitzer B, van der Meer F, Franz J, Hansen O, Stadelmann C, Salditt T. Three-dimensional virtual histology of the human hippocampus based on phase-contrast computed tomography. *Proc Natl Acad Sci U S A* 2021; **118** [PMID: 34819378 DOI: 10.1073/pnas.2113835118]
- 32 **Goodarzi N**, Akbari Bazm M, Poladi S, Rashidi F, Mahmoudi B, Abumandour MMA. Histology of the small intestine in the common pheasant (*Phasianus colchicus*): A scanning electron microscopy, histochemical, immunohistochemical, and stereological study. *Microsc Res Tech* 2021; **84**: 2388-2398 [PMID: 33908129 DOI: 10.1002/jemt.23794]
- 33 **Eckermann M**, Ruhwedel T, Möbus W, Salditt T. Towards correlative imaging of neuronal tissue by phase-contrast x-ray tomography and SEM. *Proceedings of the SPIE* 2021; **11840**: 29-36 [DOI: 10.1117/12.2596133]



Published by **Baishideng Publishing Group Inc**  
7041 Koll Center Parkway, Suite 160, Pleasanton, CA 94566, USA  
**Telephone:** +1-925-3991568  
**E-mail:** [bpgoffice@wjgnet.com](mailto:bpgoffice@wjgnet.com)  
**Help Desk:** <https://www.f6publishing.com/helpdesk>  
<https://www.wjgnet.com>

